INL-EXT-21-62113
Revision 0

Dynamic Line Rating Study of Concurrent Cooling Effects for a Proposed Wind Farm

March 2021

Changing the World's Energy Future

Alexander Abboud
Tyler Phillips
Jacob Lehmer
Brandon Starks
Jake Gentle

INL is a U.S. Department of Energy National Laboratory operated by Battelle Energy Alliance, LLC

INL-EXT-21-62113
Revision 0

Dynamic Line Rating Study of Concurrent Cooling for a Proposed Wind Farm

Alexander Abboud
Tyler Phillips
Jacob Lehmer
Brandon Starks
Jake Gentle

March 2021

Idaho National Laboratory
Idaho Falls, Idaho 83415

http://www.inl.gov

Prepared for the
U.S. Department of Energy
Wind Energy Technologies Office
Under DOE Idaho Operations Office
Contract DE-AC07-05ID14517

Page intentionally left blank

SUMMARY

This report was prepared for the Wind Energy Technology Office for the FY 2021, quarter 2 deliverable. This details the use of dynamic line rating technology to rate a gen tie-line associated with a proposed wind farm. By utilizing dynamic line rating, the concurrent cooling effect – when maximum wind farm power output is coupled with additional convective cooling on the gen tie line – can be used to provide a smaller size conductor for the gen tie line, thus reducing the capital costs.

Page intentionally left blank

CONTENTS

FIGURES

TABLES

Page intentionally left blank

ACRONYMS

CFD	Computational Fluid Dynamics
DLR	Dynamic Line Rating
GLASS	General Line Ampacity State Solver
RANS	Reynolds-averaged Navier-Stokes
TREAD	Transmission Route Engineering Analysis and Design

Page intentionally left blank

Dynamic Line Rating Study of Concurrent Cooling for a Proposed Wind Farm

1. Introduction

Transmission line ratings are given by a maximum ampacity based on the maximum conductor temperature limits, which are typically set to avoid sagging or clearance issues of the transmission line segments between structures due to thermal expansion. The dependency of maximum ampacity on the maximum temperature and weather conditions has standard models that were developed by the International Council on Large Electric Systems (CIGRE) (CIGRE 1992; CIGRE 2006; CIGRE 2014), the International Electrochemical Commission (IEC) (IEC 1985) and the Institute of Electrical and Electronics Engineers (IEEE) (IEEE 2012; IEEE 2016).

The weather conditions used in these methods are typically constant values year-round or with seasonal patterns, and are set using conservative assumptions for the conditions. By not accounting for additional cooling during periods of high wind or low ambient temperature, there is likely unused head room on many overhead transmission lines. Dynamic Line Rating (DLR) uses a changing line rating based on local conditions rather than a static rating assumption to provide additional ampacity capacity to a transmission line. DLR has been identified by the United States Department of Energy as a distribution infrastructure solution to defer upgrades, support line outages, and increase yields of distributed generation (US DOE, 2010; US DOE 2014).

The conservative nature of transmission line standards and the regional transmission operators (RTOs) can be hard to adjust, so research showing the benefits of DLR is important to prove the benefits of the method. Case studies utilizing weather data in the field has shown potential for DLR to increase ampacity above static throughout several countries (Greenwood et al., 2014; Bhattarai et al., 2017; Bhattarai et al., 2018; Usik-Joustenvuo and Pasonen, 2013; Aznarte and Siebert, 2017) Further studies have involved coupling the weather data with forecast model to be used for forecasted ratings, and assessment of risk (Abboud et al., 2019b).

This study utilizes the coupling of field weather data and weather model data from the High-resolution rapid refresh model (HRRR) within the region of interest with Computational Fluid Dynamics (CFD) results. For the wind field simulations, the steady-state Reynolds-Averaged Navier Stokes (RANS) approach was used for turbulent modelling of the wind flow (Jones and Launder, 1972). The RANS approach has been used to validate wind flows in complex terrains (Wallbank, 2008) with adequate speed up predictions (Dhunny et al., 2016) and low-elevation mountains within acceptable error (Dhunny et al., 2015; Dhunny et al., 2017). Due to the convective cooling calculation, the error in the cooling rate scales as approximate the square root of the wind speed, so a 10% error in wind speed is only a 5% error in the cooling rate. The site of interest in just outside of the Idaho National Laboratory property boundary in eastern Idaho, with a domain extent of 40 km by 40 km.

The weather forecasts used in this study came from version 3 of the HRRR model. HRRR is a convection-allowing forecast model that outputs meteorological variables on a 3-km horizontal grid over the continental United States (Benjamin et al., 2016; Smith et al., 2008).The HRRR was developed at the National Oceanic and Atmospheric Administration (NOAA) Earth System Research Laboratory and is run operationally at the National Center for Environmental Prediction (NCEP). The previous version of the HRRR, Version 3, became operational on 12 July 2018 and outputs forecasts from zero through 18 hours with 15-minute temporal resolution that are updated every hour. The model also outputs forecasts from zero to 36 hours with one-hour temporal resolution at 00, 06, 12, and 18 UTC. While the HRRR version 4 recently became operational and allows for 48 hour forecasts, this was only in December 2020, so not enough data is available yet.

In addition to transmission lines for regional power, another benefit to DLR is concurrent cooling effects associated with wind farms. With higher wind speeds, the power generation of wind farms increases at the same time that the ampacity of a transmission line is increased due to higher cooling rates. This effect could be used to avoid curtailment of power generation, and some studies have proved this correlation (Cao et al., 2016; Talpur et al., 2015, Banerjee et al., 2015). Here, we seek to expand the research by looking at the rating of a transmission line prior to the construction to select a proper conductor with DLR in mind. Figure 1 shows the region of interest of the proposed wind farm. This map contains the rows of turbines marked with the flags along with the lettering/numbering of each. The two push pins denote the approximate locations of the collector substations. The proposed gen tie line would run parallel to highway 20 in the map. In the CFD model, the underperforming wind turbines are cut out of this initial plan, and only the most efficient turbines are utilized.

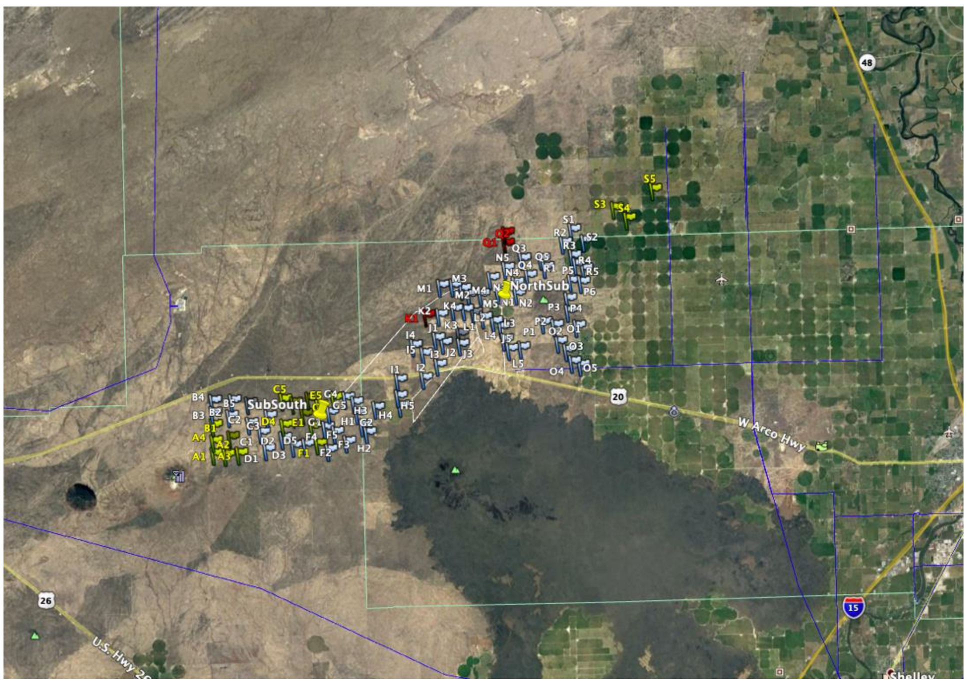

Figure 1. The region of interest for the wind farm.

This report describes the methodology used for the DLR calculations, shows the domain model of the region that is used, discusses the dynamic line rating results and concurrent cooling effects based on the wind power generation, and finally shows an example of the TREAD routing tool developed at INL.

2. Methodology

2.1 Line Rating

The equations for DLR are the same used for static rating, based on a simple heat balance for a transmission line. For the weather data, the output is at 5-minute intervals. For the HRRR model data the data output is only done in hourly intervals. The heat balance equation is used to solve for the maximum current, *I*, to get (IEEE, 2012)

$$I = \sqrt{\frac{q_c + q_r - q_s}{R(T_c)}} \tag{1}$$

Where q_c, q_r, and q_s are the convective, radiative and solar contributions, and R is the conductor resistance as a function of the conductor temperature T_c. The radiated heat loss per unit length in units of W/m is given by

$$q_r = 17.8D\epsilon\left[\left(\frac{T_c + 273.15}{100}\right)^4 - \left(\frac{T_a + 273.15}{100}\right)^4\right] \tag{2}$$

Where ϵ is the emissivity, T_a is the ambient air temperature and D is the conductor diameter. The heat gain through solar irradiance is given by

$$q_s = \alpha Q_{se}\sin(\theta)A' \tag{3}$$

Where α is the solar absorptivity, Q_{se} is the total solar and sky radiated heat flux corrected by elevation, θ is the effective angle of incidence of the sun's rays and A' is the projected area of the conductor. The convective heat loss is calculated using one of three equations for high wind speeds, low wind speed (below 3 mph) or natural convective cooling. For high wind speed the equation is given by

$$q_{c1} = \left[1.01 + 1.35\left(\frac{DV_w\rho_f}{\mu_f}\right)^{0.52}\right]k_f K_{angle}(T_c - T_a) \tag{4}$$

For low wind speed the equation is given by

$$q_{c2} = 0.754\left(\frac{DV_w\rho_f}{\mu_f}\right)^{0.6} k_f K_{angle}(T_c - T_a) \tag{5}$$

Or for natural convection the equation is given by

$$q_{cn} = 3.645\rho_f^{0.5}D^{0.75}(T_c - T_a)^{1.25} \tag{6}$$

Where V_w is the speed of air, with fluid parameters density ρ_f, viscosity μ_f and thermal conductivity k_f calculated at the ambient temperature. And K_{angle} is the wind direction factor which can vary from about 0.3 to 1.0 based on parallel or perpendicular wind flow to the transmission line, given by

$$K_{angle} = 1.194 - \cos(\phi) + 0.194\cos(2\phi) + 0.368\sin(2\phi) \tag{7}$$

Where ϕ is the angle of incidence between the wind and the transmission line midpoint. The GLASS code developed by INL does all of these calculations for every single transmission line midpoint of interest. The minimum value among all the midpoint calculations is assumed to be the ampacity for each line.

For the gen-tie line of interest, it is assumed that the voltage is 161 kV. The maximum conductor temperature for the rating is 75 C, with an emissivity and absorptivity both equal to 0.5. For the static rating, the constant weather parameters assumed a wind speed of 2 ft/sec perpendicular to the conductor, 25 C ambient temperature, and 96 W/ft^2 solar irradiation.

Then static rating is used to determine the baseline for the conductor size that is needed for the total power of the wind farm. The dynamic line rating for each of the smaller conductors is calculated then used in Eq 8 to determine the total power carrying capacity of the gen tie line.

$$P = (3)IV \tag{8}$$

2.2 Computational Fluid Dynamics

The CFD domain is set up as shown in Figure 2. Figure 2a shows the elevation map with the wind turbine locations, 2b shows the roughness layer, 2c shows gen-tie line 1, and 2d shows gen tie-line 2. The elevation map scale is in meters showing low areas and green, and high areas, such as nearby buttes in brown. The roughness layer shows regions of low to high vegetation and cities where near ground wind fields would be affected. These regions are not explicitly modelled in the CFD, so the roughness layer is used to approximate slowdowns due to these subgrid effects. This value is set to 1.0 for city regions (dark red on the scale), 0.8 for heavily forested areas (red on the scale), 0.1 - 0.2 for farmland or plains covered in shrubs (yellow on the scale), and set to 0 (white on the scale) for flat areas, such as along the water surface, and for areas with very little vegetation. The roughness values are used in the log- law correlations for the boundary layer with values adapted from Troen and Petersen, 1989. This wind farm is set up for a total of 78 turbine locations with a total output of 450 MW. The first gen tie line runs from the collector for the southwestern turbines up to the collector for the northeastern cluster of turbines. It is assumed that the total power output is split in half such that this line carries a maximum 225MW. The second gen tie line runs from this northeastern collector along the highway out to the main regional transmission lines. The end point is at a transformer station along the regional transmission lines which already exists.

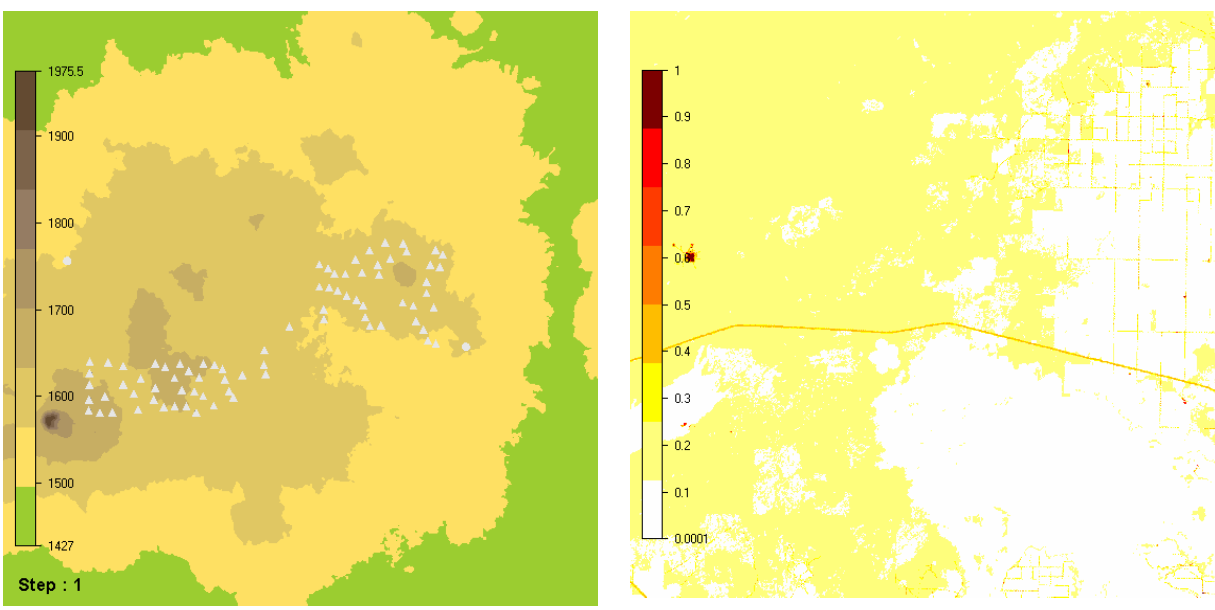

(a) (b)

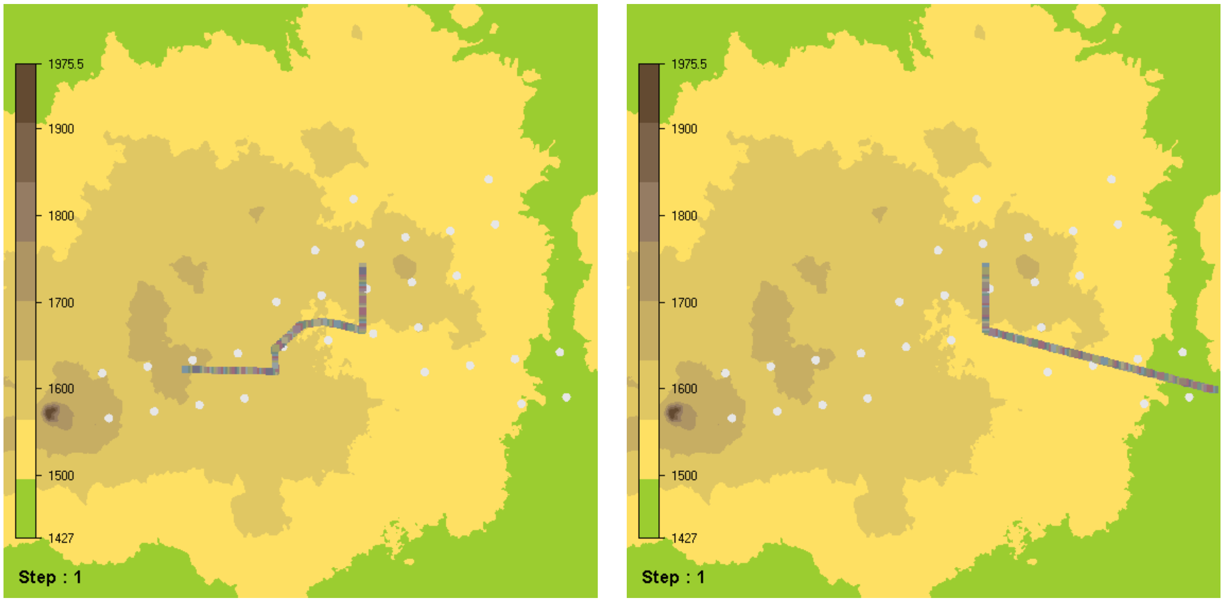

(c) (d)

Figure 2. The region of interest for the wind farm with (a) wind turbine layout, (b) roughness layer, (c) gen tie line 1 and (d) gen tie-line 2.

The CFD domain consists of 40 million computational cells, with 40-meter spatial resolution in the horizontal direction and varying spatial resolution vertically. The vertical resolution is spaced such that near the ground the resolution is in 5-meter increments to allow for accurate wind fields near the transmission lines, while above 100 meters a log scale is used up to the atmospheric boundary layer.

The steady-state standard *k*-ε RANS model is used for modelling the turbulent kinetic energy and dissipation rate. The PDEs for the solution consist of the velocity vectors, the continuity equation, and equations for the turbulent kinetic energy and turbulent dissipation rates. The equation for the velocity vectors is

$$\rho U_i \frac{\partial U_j}{\partial x_i} = \frac{\partial}{\partial x_i}\left[(\mu + \mu_t)\left(\frac{\partial U_i}{\partial x_j} + \frac{\partial U_j}{\partial x_i}\right)\right] - \frac{\partial p}{\partial x_i} \tag{9}$$

The turbulent kinetic energy, *k*, equation is given by

$$\frac{\partial (U_i k)}{\partial x_i} = \frac{\partial}{\partial x_i}\left[\frac{\mu_t \partial k}{\sigma_k \partial x_i}\right] + P_k - \epsilon \tag{10}$$

And the equation for the turbulent dissipate rate, , is given by

$$\frac{\partial (U_i \epsilon)}{\partial x_i} = \frac{\partial}{\partial x_i}\left[\frac{\mu_t \partial \epsilon}{\sigma_\epsilon \partial x_i}\right] + c_{\epsilon 1}\frac{\epsilon}{k}P_k - c_{\epsilon 2}\frac{\epsilon^2}{k}P_k \tag{11}$$

Where the turbulent viscosity, is given by

$$\mu_t = \frac{C_\mu k^2}{\epsilon} \tag{12}$$

And the turbulent production term, is given by

$$P_k = \mu_t \left(\frac{\partial U_i}{\partial x_j} + \frac{\partial U_j}{\partial x_i} \right) \frac{\partial U_i}{\partial x_j} \tag{13}$$

Where c_μ, c_{ϵ_1}, c_{ϵ_2}, σ_k, and σ_ϵ and are the fixed constants for the model, with values set to 0.09, 1.55, 2.0, 1.0, and 1.3, respectively (Jones and Launder, 1972).

2.3 TREAD

INL’s Transmission Route Engineering Analysis and Design [tool] (TREAD) is a tool meant for the design and routing of new transmission lines. This software takes care of much of the tedious work required to plan a new transmission line. It is capable of creating the plan for a transmission line that has been optimized for a single or multiple different values. TREAD is capable of taking an arbitrarily large amount of surface layers represented as geographical files and then using a modified version of Dijkstra’s Algorithm for finding the best path based on what data is available and what has been determined to be valuable.

These different shape files represent real world geometry and have associated values for various heuristic factors. These heuristic factors are such things as the cost of building on the land or adjacency to areas. The combination of these different heuristics will create a series of routes through the provided area that have been optimized for many different factors depending on what is required for the situation at hand.

The system uses the base principle behind Dijkstra’s Algorithm with an infinite implied radial grid. This design choice allows for an arbitrarily large space that does not require defining rectangular resolution or boundary areas. The system is capable of running on any system that is capable of running a Java virtual machine. TREAD is also capable of interacting with different weather models in order to gather weather data about the locations that are being routed to.

This weather data is then used in conjunction with INL’s General Line Ampacity State Solver to optimize the conductor for concurrent cooling or localize hot spots and then give a conductor recommendation that solves the hotspot. This process is able to happen iteratively or a single time. TREAD allows the user to graphically interact with this system and visualize, in real time, the routing that might take place. There is an arbitrary range between manual route creation and automatic route creation. Manual route creation gives the opportunity to hand design routes and test the choices with computer generated routes along the same shape files.

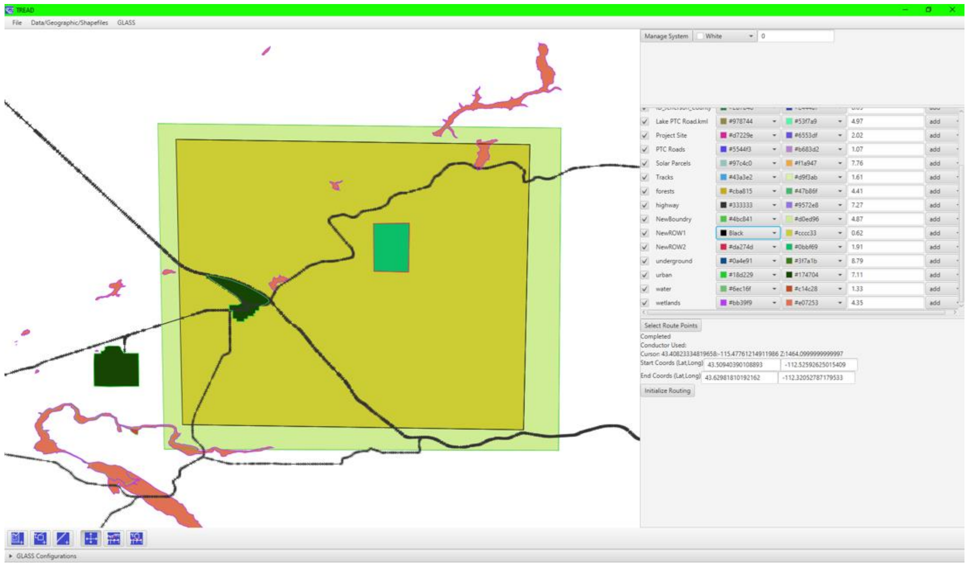

Figure 3. Example TREAD image.

3. Results

3.1 Weather Station Data/Computational Fluid Dynamics

Respectively, figures 4a and 4b show distributions of wind data collected from 2018 to 2020 by the Kettle Butte weather station (latitude: 43.547, longitude: –112.326) and the nearest set of HRRR 3-hour forecasted data (latitude: 43.532, longitude: –112.322). These distributions show that near-term predictions are in agreement with observed wind conditions, having similar profiles. The most notable difference between the two distributions is that forecasts predict more wind currents traveling south than what was recorded in observational data, though the difference is minimal overall.

Figures 4c and 4d respectively show diurnal profiles of solar and temperature data collected by KET and the nearest set of HRRR 3-hour forecasted data. The yearly trend observed in the two data sets are very similar, having closely related envelopes with respect to daily maxima of solar and temperature values, though weather observations show more erratic maxima throughout the year than what is predicted in forecasts. This has a lesser impact on the DLR of the gen tie line compared to other weather quantities (e.g., wind speed or direction).

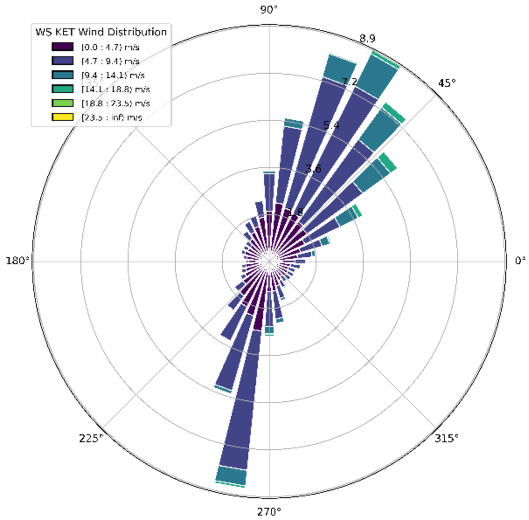

(a)

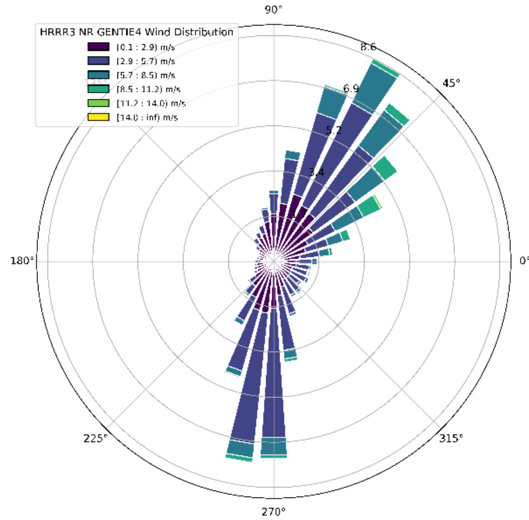

(b)

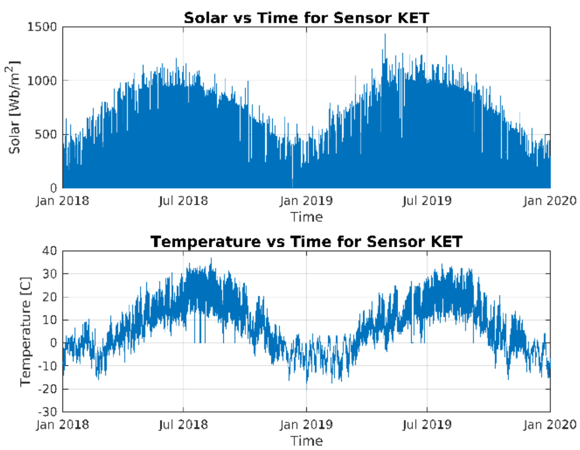

(c)

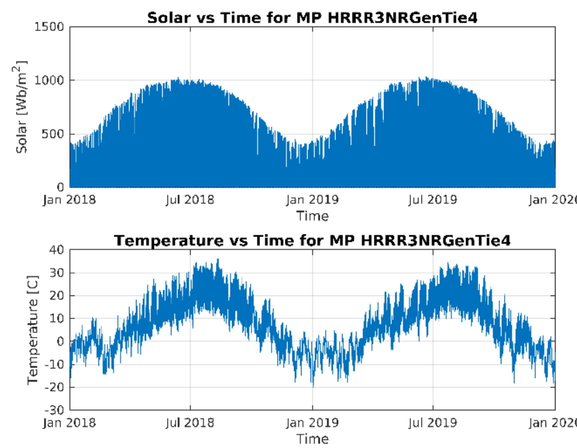

(d)

Figure 4. The Kettle Butte weather station data wind statistics (a) and diurnal profiles (b) compared to the closest HRRR model point wind statistics (b) and diurnal profiles (d).

Five statistical tests were performed to assure the integrity of the weather data used, and consequently the DLR ratings. These tests consisted of checking the entire data set for wind speeds greater than 75 m/s (test 1), wind speed changes less than 0.5 m/s/hour (test 2), subsequently constant wind direction entries with varying speed (test 3), wind speed changes greater than 20 m/s (test 4), and temperature changes greater than 8°C/hour (test 5).

Each entry in the KET data was recorded approximately every five minutes. Tests 1-5 yielded percentage discrepancies of 0.00%, 6.2%, 0.74%, 0.00%, and 0.11%, respectively. These results show good overall qualities of the data, though the outstanding figure of 6.2% for the sustained wind speeds per hour can be most likely attributed to periods of low wind currents. Tests 1-5 were also performed on the forecasted data to observe differences between observational and forecasted data, but because the forecasted data was given each hour, test 2 was neglected. These four tests yielded no percentage discrepancies which is in close agreement to tests 1, 3, 4, and 5 for the KET data set.

The results for the CFD wind fields are shown in Figure 5 for the domain of interest. The data shown is for the north, east, south and west incoming wind vectors. There are eight additional sectors models at 30 degree spacing, but these are left out for brevity. The wind data is shown at two different heights, 10-meters above ground level – corresponding to the height of the transmission lines, and at 115-meters above ground level – corresponding to the hub heights of the wind turbines. The wind profile is less affected by the terrain at the higher elevations of the turbines.

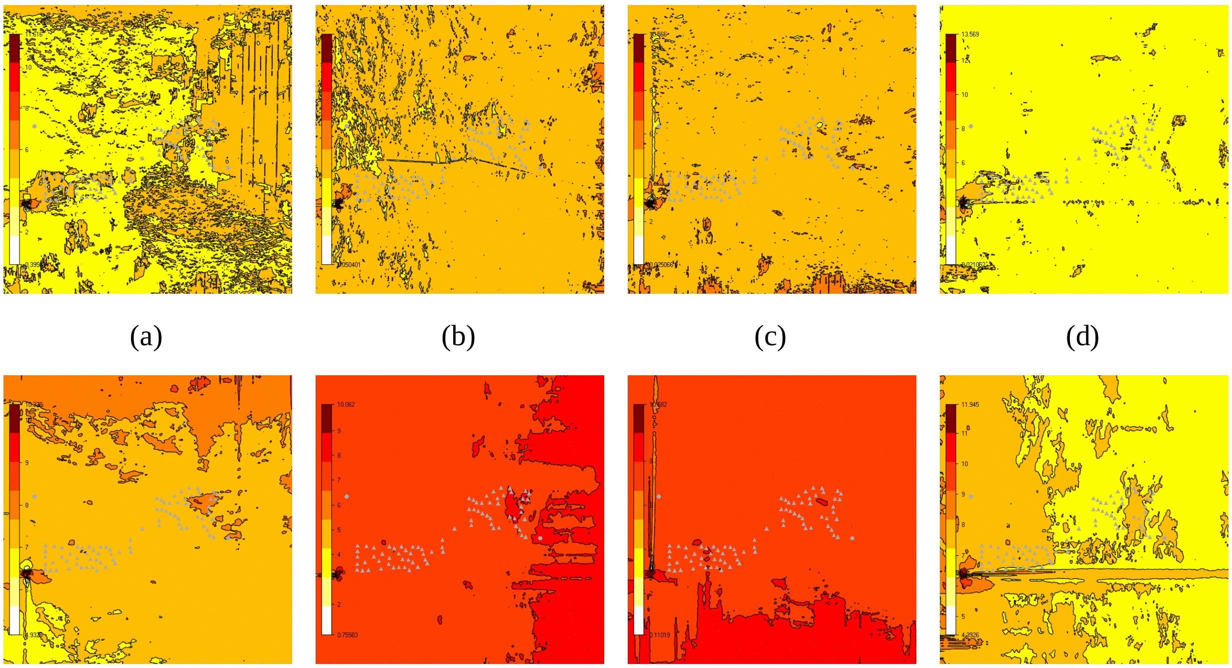

(a) (b) (c) (d)

(e) (f) (g) (h)

Figure 5. The CFD results for the heights corresponding to the gen tie lines for incoming (a) north, (b) east, (c) south and (d) west incoming wind, and the CFD results for the heights corresponding to the wind turbines for incoming (e) north, (f) east, (g) south and (h) west incoming wind.

3.2 Wind Farm Power Generation

The turbines at the proposed wind farm are assumed to be Siemen-Gamesa 5.8 MW turbines. Their power curve is shown in Figure 6, with the black dotted lines. The cut-in speed starts at 3.5 m/s, and starts to cut out at 21 m/s, before generation stops above 26 m/s. The red line in Figure 6 shows the thrust coefficient.

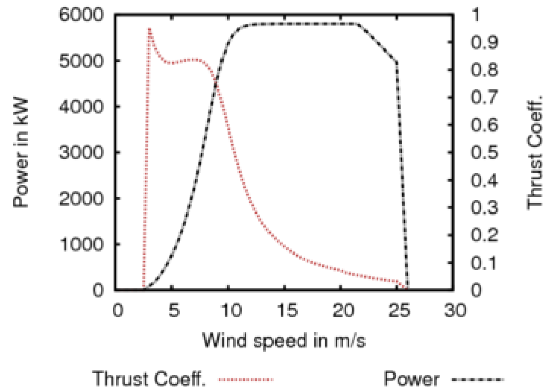

Figure 6. SG power generation curve.

This power curve is used for the power generation of the turbines shown in Figure 1. They are split equally into two sites. Site 1 is in the turbines in the southwest and has a maximum generation of 225 MW. Site 1 is connected to site 2 by gen tie-line 1. Site 2 is in the north east and gen tie-line 2 carries a maximum generation of 450 MW. Figure 7 shows a week-long period of wind generation at each site and the total generation. This figure also shows the static line rating for gen tie-line 1 and 2 using the base line conductor of ACSR Partridge and Bluejay, respectively. These conductors allow for the maximum power output of the wind farm. The static capacity was determined using the static weather conditions given in Section 2.1. This results in ampacity of 475 and 1,092 amps for the lines, respectively. The lines have a voltage of 161,000 and this results in a static power rating for the gen tie-lines of 230 and 528 MW, respectively.

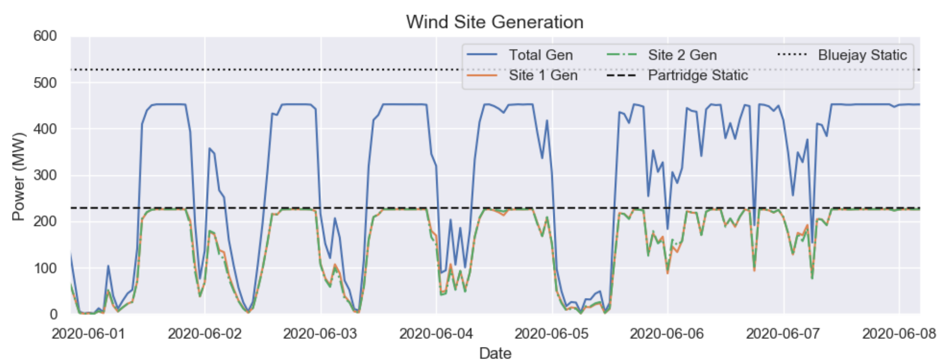

Figure 7. Wind Generation at sites 1 and 2, as well as the total generation. The static power rating of each gen tie-line is also shown.

3.3 Dynamic Line Rating

The dynamic line rating is calculated in ampacity. To evaluate the conductor transmission capacity in megawatts Equation 8 is used and referred to as the dynamic power capacity. The results of the dynamic power capacity of the baseline conductor Ibis in gen tie-line 1 over a week-long period is shown by the top plot in Figure 8. Here, the power flow is shown as calculated by the weather station data and the HRRR3 and HRRR36 models. The bottom plot is the dynamic power capacity error for each one of the models over the same timeframe. The error is calculated as

$$error = P_{HRRR} - P_{WS}$$

Where P_{HRRR} is the power results of the HRRR3 or HRRR36 forecast and P_{WS} is the power calculated from the weather station. Therefore, a positive value represents when the forecast model over predicts the power capacity of the line.

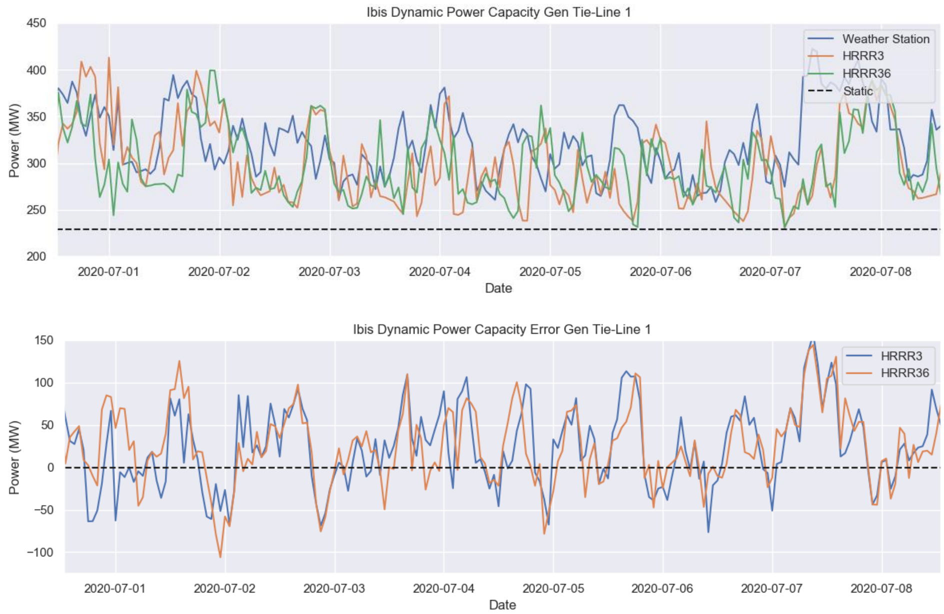

Figure 8. Dynamic power capacity (top) and error of HRRR3 and HRRR36 (bottom) over a week-long period using baseline Ibis conductor on gen tie-line 1.

Using the error of the models the root mean squared error is calculated as

$$RMSE = \sqrt{\frac{\sum_{i=1}^{N}(P_{HRRR} - P_{WS})^2}{N}}$$

where N is the number of data points. The results of the RMSE for both tie-lines are given in Table 1. Due to different capacity of different conductors the percent error is calculated as

$$\%\,error = \frac{|P_{HRRR} - P_{WS}|}{P_{WS}} * 100$$

This value is the used in the RMSE to replace the error resulting in a %RMSE, given mathematically as

$$\%RSME = \sqrt{\frac{\sum_{i=1}^{N}\left(\frac{P_{HRRR} - P_{WS}}{P_{WS}} * 100\right)^2}{N}}$$

Table 1. Dynamic power capacity RMES and %RMSE for potential conductors on each gen tie-line.

	Conductor	HRRR3		HRRR36	
		RSME	%RSME	RSME	%RSME
Gen Tie Line 1	Ibis	55.0	15.2	55.0	15.4
	Partridge	54.2	15.6	43.2	15.8
	Pigeon	30.4	16.1	30.5	16.3
Gen Tie Line 2	Bluejay	153.0	19.1	151.8	19.3
	Snowbird	145.8	19.2	144.7	19.4
	Drake	127.4	19.4	126.5	19.6
	Gull	112.1	19.6	111.3	19.8
	Ibis	82.9	20.0	82.4	20.2

3.4 Concurrent Cooling

The concurrent cooling effect is the analysis of how much additional power capacity is available on the gen tie-line compared to the wind generation power. A week-long period of wind generation and dynamic line rating using the baseline conductor is shown in Figure 9. Here, the concurrent cooling in the top plot is defined as the Partridge DLR – Site 1 Gen.

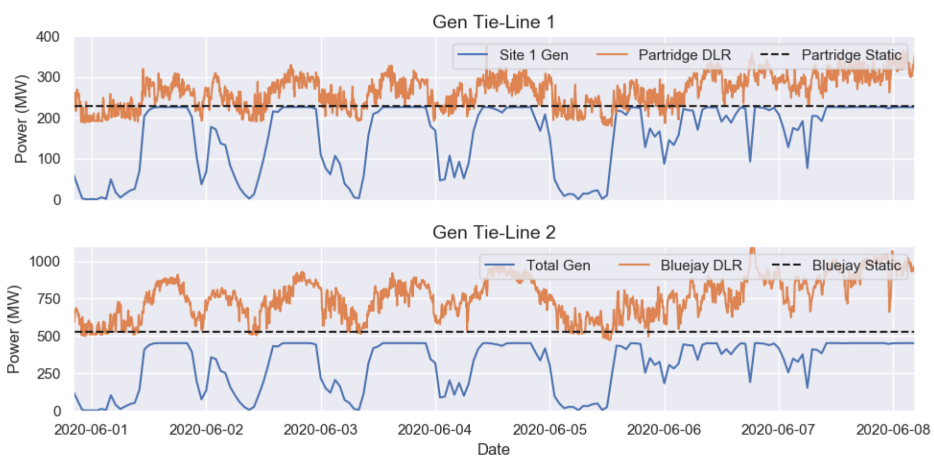

Figure 9. Concurrent Cooling of the wind generation and dynamic power capacity.

The concurrent cooling is calculated over the calendar year 2020 using the baseline conductor as well as ACSR Ibis and Pigeon for gen tie-line 1 and ACSR Snowbird, Drake, Gull, and Ibis for gen tie-line 2. The results are sorted and shown in Figure 9. Here, the percent of time and additional capacity on each line based on different conductors is clear. For example, the power capacity of a Pigeon conductor for gen tie-line 1 is below the site 1 generation 78% of the time. Furthermore, the baseline conductor Partridge exceeds it 100% of the time and has a minimum additional capacity of 3 MW, while the Ibis conductor has a minimum additional capacity of 69 MW. The results are further detailed in Table 2.

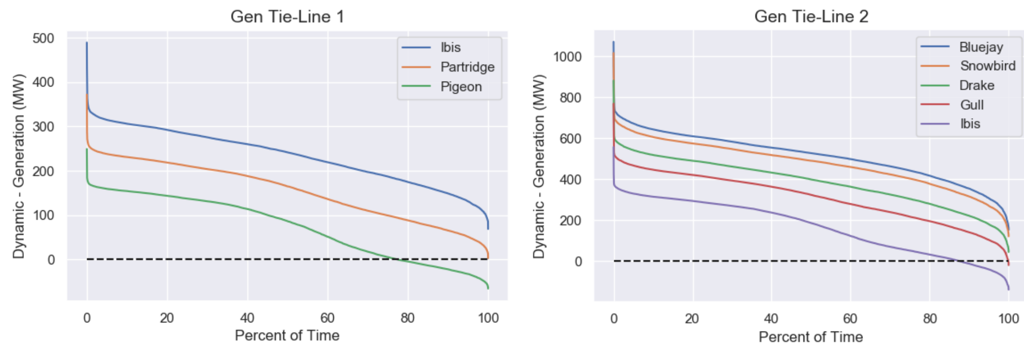

Figure 9. Access power capacity vs. percent of time using the dynamic power capacity.

Table 2. Concurrent cooling Summary.

	Conductor	Percent of Time 80%	90 %	95%	99%	100%
Gen Tie Line 1	Ibis	175	149	131	105	68
	Partridge	89	66	51	31	3
	Pigeon	-4	-21	-32	-49	-65
Gen Tie-Line 2	Bluejay	417	354	307	233	153
	Snowbird	377	316	270	199	122
	Drake	280	221	180	116	45
	Gull	196	141	104	48	-19
	Ibis	32	-12	-40	-83	-138

For the cost of the gen-tie line, a simple analysis can be done on the cost of the conductor itself. Online calculators (https://www.wireandcableyourway.com/acsr-aac-aaac) are available to estimate the cost of ACSR conductors on a $/length basis. The total length of gen-tie line 1 is 18253 m, and the total length of gen-tie line 2 is 19916 m. For gen-tie line 1, the approximate cost for these lines in Table 1 is then $95,220, $114,983, and $41,322 for the Ibis, Partridge and Pigeon lines. The Pigeon line could provide a conductor with minimal curtailment at a savings of $74,000. For the gen-tie line 2, the approximate costs are $262,682, $219,555, $196,685, $146,370, $103,896 for Bluejay, Snowbird, Drake, Gull and Ibis conductors. Thus, for the second gen tie with 450 MW capacity, by utilizing DLR on the ampacity, the conductor used could be a Drake instead of a Bluejay, with no generation that would need to be curtailed, for a potential savings in construction of about $65,000. If management of the real time ampacity were coupled with curtailment of the wind and possible regional capacity, further savings could be achieved through construction of a Gull conductor for curtailment less than 1% of the time or an Ibis conductor with curtailment about 10% of the time, for cost savings of about $115,000 and $160,000 for the conductor of the gen tie line.

3.5 TREAD Results

The output from the TREAD system is shown below in figure 9. The route shown makes roughly a straight line towards the main road running through the area and then proceeds to follow this road until reaching the transmission tie point. This is an expected result for a setup like this, looking at how the area is organized will usually result in a line that the system will follow. Humans are especially good at image processing and pattern recognition, both of which is used in a routing algorithm. This usually yields a route which people would call intuitive.

The data set available to generate this route is quite small with very few depth of layers. This is one of the contributions to a highly intuitive route. The TREAD system demonstrates its value of when dealing with multiple overlapping shape files that would be tedious to look up by hand and find the value that influences the routing. With TREAD there is not theoretical limit to the number of layers that could be used and the costing function that could be applied.

In even the most complex of systems often times the routes appear very intuitive. The primary cause of this is that straight lines are always the least expensive way to route points, the routing process becomes less about finding a unique way through large obstacles but rather finding the easiest point to route through and then creating a series of these points to wherever they need to go, this once again creates a simple and intuitive path.

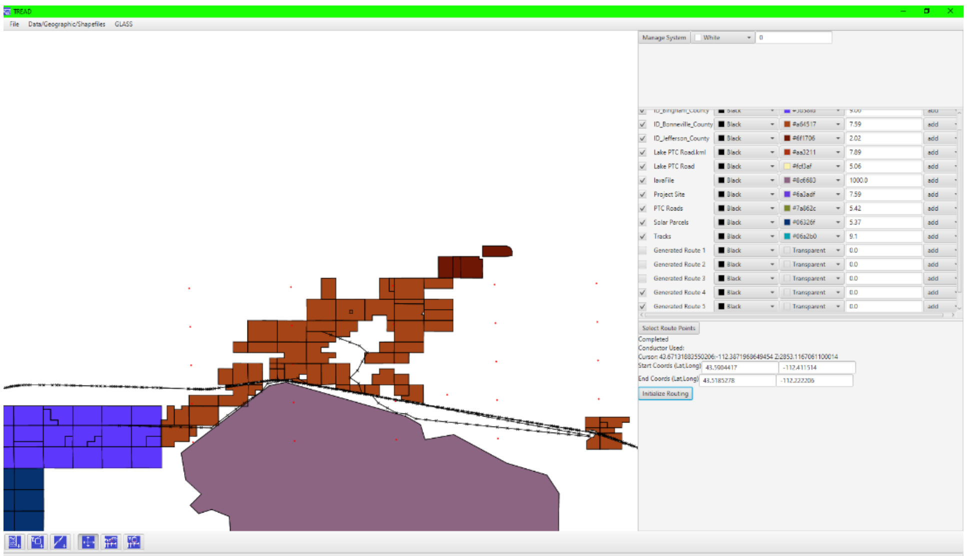

Figure 10. TREAD plots.

REFERENCES

Abboud, Alexander W., Kenneth R. Fenton, Jacob P. Lehmer, Benjamin A. Fehringer, Jake P. Gentle, Timothy R. McJunkin, Katya L. Le Blanc, Melissa A. Petty, and Matthew S. Wandishin. "Coupling computational fluid dynamics with the high resolution rapid refresh model for forecasting dynamic line ratings." *Electric Power Systems Research* 170 (2019a): 326-337.

Abboud, Alexander W., Jake P. Gentle, Timothy R. McJunkin, and Jacob P. Lehmer. "Using Computational Fluid Dynamics of Wind Simulations Coupled with Weather Data to Calculate Dynamic Line Ratings." *IEEE Transactions on Power Delivery* 35, no. 2 (2019b): 745-753.

B. J. L. Aznarte and N. Siebert, “Dynamic line rating using numerical weather predictions and machine learning: A case study,” IEEE Trans. Power Delivery, vol. 32, no. 1, pp. 335–343, 2017.

B. Banerjee, D. Jayaweera, S. Islam. “Risk constrained short-term scheduling with dynamic line ratings for increased penetration of wind power.” Renew Energy, 83 (2015), pp. 1139-1146.

S. G. Benjamin, S. S. Weygandt, J. M. Brown, M. Hu, C. R. Alexander, T. G. Smirnova, J. B. Olson, E. P. James, D. C. Dowell, G. A. Grell, et al., A north american hourly assimilation and model forecast cycle: The rapid refresh, Mon. Weather Rev. 144 (2016) 1669–1694.

B. P. Bhattarai, J. P. Gentle, P. Hill, T. McJunkin, K. S. Myers, A. Abboud, R. Renwick, and D. Hengst, “Trans- mission line ampacity improvements of altalink wind plant overhead tie-lines using weather-based dynamic line ratings,” in IEEE PES General Meeting, July 2017.

B. P. Bhattarai, J. P. Gentle, T. McJunkin, P. J. Hill, K. Myers, A. Abboud, and D. Hengst, “Improvement of transmission line ampacity utilization by weather-based dynamic line ratings,” IEEE Transactions on Power Delivery, 33(4), pp 1853-1863.

J. Cao, W. Du, H.F. Wang. “Weather-based optimal power flow with wind farms integration.” IEEE Trans Power Syst, 31 (4) (2016), pp. 3073-3081

CIGRE Working Group 22.12, “The thermal behaviour of overhead line conductors,” Electra, vol. 114, no. 3, pp. 107–125, 1992.

“Guide for selection of weather parameters for bare overhead conductor ratings,” CIGRE WG 22.12, Tech. Rep., 2006.

“Guide for thermal rating calculations of overhead lines,” CIGRE WG B2.43, Tech. Rep., 2014.

D. Greenwood, J. Gentle, K. Myers, P. Davison, I. West, J. Bush, G. Ingram, and M. Troffaes, “A comparison of real-time thermal rating systems in the U.S. and the U.K.” IEEE Trans. Power Delivery, vol. 29, no. 4, pp. 1849– 1858, August 2014.

“Overhead electrical conductors calculation methods for stranded bare conductors,” IEC Standard TR 1597, Tech. Rep., 1985.

“Standard for calculating current-temperature relationship of bare overhead line conductors,” IEEE Standard 738, Tech. Rep., 2012.

IEEE PES WG Subcommittee 15.11, “Real-time over- head transmission line monitoring for dynamic rating,” IEEE Transactions on Power Delivery, vol. 31, no. 3, 2016.

W. Jones and B. Launder, “The prediction of laminarization with a two-equation model of turbulence,” International journal of heat and mass transfer, vol. 15, no. 2, pp. 301–314, 1972.

T. Smith, S. Benjamin, J. Brown, S. Weygandt, T. Smirnova, B. Schwartz, Convection forecasts from the hourly updated, 3-km high resolution rapid refresh (hrrr) model., in: 24th Conference on Severe Local Storms, Savanah, GA, 2008.

S. Talpur, C.J. Wallnerstrom, C. Flood, P. Hilber. “Implementation of dynamic line rating in a sub-transmission system for wind power integration.” Smart Grid Renew Energy, 6 (8) (2015), pp. 233-249

I. Toren and E. L. Petersen, European Wind Atlas. Risø National Laboratory, 1989.

“Dynamic line rating systems for transmission lines: American recovery and reinvestment act of 2009,” U.S. Department of Energy, Tech. Rep., 2014.

“Smart grid system report,” U.S. Department of Energy, Tech. Rep., 2010.

S. Uski-Joutsenvuo and R. Pasonen, “Maximizing power line transmission capability by employing dynamic line ratings technical survey and applicability in finland, vtt- r-01604-13,” Tech. Rep., 2013.

https://www.wireandcableyourway.com/acsr-aac-aaac